

# Time-Domain Boundary Element Method with Broadband Impedance Boundary Condition

Michelle E. Rodio\*

NASA Langley Research Center, Hampton, Virginia 23681

Fang Q. Hu†

Old Dominion University, Norfolk, Virginia 23529

and

Douglas M. Nark‡

NASA Langley Research Center, Hampton, Virginia 23681

https://doi.org/10.2514/1.J060614

Acoustic liners are an effective tool for noise reduction and are characterized by a frequency-dependent impedance value. In this paper, a time-domain boundary element method for acoustic scattering coupled with a broadband impedance boundary condition is studied for the case of no mean flow. A Burton-Miller reformulation of the time domain boundary element method for acoustic scattering is carried out with both the pressure and its surface normal derivative terms retained. A multipole impedance model is converted into the time domain and used for enforcing an impedance boundary condition over a wide range of frequencies. Discretization of the coupled system is described. In particular, the time-domain impedance boundary condition is discretized by the third-order implicit backward difference scheme. Stability of the coupling is assessed by an eigenvalue analysis. Scattering solutions that demonstrate the validity and stability of the numerical method are presented.

#### I. Introduction

FTHODS for deriving an integral equation for the prediction of acoustic scattering have been studied extensively in both the frequency and time domains (e.g., see Refs. [1–4]). Frequency-domain solvers are the most used and researched within the literature; they have a reduced computational cost, allow for modeling time-harmonic fields at a single frequency, avoid the growth of Kelvin–Helmholtz instability waves, and allow for an impedance boundary condition to be imposed directly. Despite these benefits, there are several distinct advantages to using a time-domain solver [5]. Time-domain solvers allow for the simulation and study of broadband sources and time-dependent transient signals. Time-domain solvers also allow for the scattering solution at all frequencies to be obtained within a single computation and avoid needing to invert a large dense linear system as is required in the frequency domain. Moreover, a time-domain solution is more naturally coupled with a nonlinear computational fluid dynamics simulation of noise sources.

Although time-domain boundary integral equations (TD-BIEs) are known to have an intrinsic numerical instability as a result of "the existence of internal modes of resonance of the body, which correspond to time harmonic solutions of the integral equation" [6], recent works have shown that a Burton–Miller reformulation of the TD-BIE can effectively eliminate the numerical instability [5,7–9]. In Ref. [5], a Burton–Miller reformulated TD-BIE was presented for acoustic scattering by rigid bodies under a uniform mean-flow assumption. In this paper, Burton–Miller reformulation is carried out for scattering by lined bodies in the case of no mean flow. Both the

pressure and its surface normal derivative terms are retained in the derivation for application of a liner impedance boundary condition.

This study is an extension of previous work by the authors [10]; the objective was to investigate feasibility for modeling acoustic wave scattering using a Burton-Miller reformulated TD-BIE when coupled with an impedance boundary condition applied on the scattering surface. Typically composed of an array of Helmholtz resonators arranged in a honeycomb structure for support and covered with a perforate face sheet, acoustic liners dissipate the incident acoustic wave and are very effective at absorbing sound [11]. The acoustic property of a liner is characterized by impedance in the frequency domain. Transformed into the time domain using Fourier transforms, an impedance boundary condition may be coupled with the TD-BIE to model acoustic scattering by lined surfaces. In Ref. [12], Li et al. developed a model to represent liner impedance along a wide range of frequencies, where the linearized Euler equations were solved by a finite difference scheme. The model was derived from the multipole impedance model in Ref. [13] and was further studied in the works of Dragna et al. [14] and Troian et al. [15]. This broadband model, satisfying the requirements of causality, reality, and passivity [16,17], will be used in the present study.

The remainder of this paper is outlined as follows. In Sec. II, the governing TD-BIE with no mean flow and its Burton–Miller reformulation with liner impedance boundary condition is provided. Next, Sec. III discusses the time-domain multipole impedance boundary condition model to be coupled with the boundary integral equation. Numerical discretization methodology for the boundary integral equation and impedance boundary condition is then provided in Sec. IV. In Sec. V, numerical stability is assessed by an eigenvalue analysis, and numerical examples of a point-source reflection by a lined sphere and by a lined flat plate are presented in Sec. VI. Concluding remarks are discussed in Sec. VII.

#### II. TD-BIE and Its Burton-Miller Reformulation

The focus of the current study is the time-domain boundary element method for acoustic scattering when coupled with an impedance boundary condition and to assess numerical stability of the coupling. Herein, a derivation of the time-domain boundary integral is provided, where both the pressure and its surface normal derivative terms are retained. Only the simple case of no mean flow is considered.

Acoustic disturbances, assumed to be of small amplitude, are governed by the linear wave equation. With no mean flow, the governing equation is given to be

Presented as Paper 2020-2547 at the 26th AIAA/CEAS Aeroacoustics Conference (AIAA Aviation 2020 Forum), Virtual, June 15–19, 2020; received 6 February 2021; revision received 28 December 2021; accepted for publication 29 December 2021; published online 16 February 2022. This material is declared a work of the U.S. Government and is not subject to copyright protection in the United States. All requests for copying and permission to reprint should be submitted to CCC at www.copyright.com; employ the eISSN 1533-385X to initiate your request. See also AIAA Rights and Permissions www.aiaa.org/randp.

<sup>\*</sup>Computational AeroSciences Branch; currently HPC Developer Operations, NextSilicon; michelle.rodio@nextsilicon.com. Member AIAA.

<sup>&</sup>lt;sup>†</sup>Professor, Department of Mathematics and Statistics; fhu@odu.edu. Associate Fellow AIAA.

<sup>&</sup>lt;sup>‡</sup>Senior Research Scientist, Structural Acoustics Branch; douglas.m.nark@nasa.gov. Associate Fellow AIAA.

$$\frac{\partial^2 p}{\partial t^2}(\mathbf{r}, t) - c^2 \nabla^2 p(\mathbf{r}, t) = q(\mathbf{r}, t)$$
 (1)

where  $\mathbf{r} = (x, y, z)$  is an arbitrary point in three-dimensional space,  $\nabla = (\partial/\partial x, \partial/\partial y, \partial/\partial z)$  and  $\nabla^2 = \nabla \cdot \nabla$ ,  $p(\mathbf{r}, t)$  is the acoustic pressure,  $q(\mathbf{r}, t)$  is the known acoustic source, and c is the speed of sound; homogeneous initial conditions are assumed,  $p(\mathbf{r}, 0) = \partial p/\partial t(\mathbf{r}, 0) = 0$ . The solution of Eq. (1) is dependent on the boundary conditions applied on the scattering surface S.

The derivation of the TD-BIE from Eq. (1) is facilitated by introducing a free-space adjoint Green's function  $\tilde{G}(\mathbf{r}, t; \mathbf{r}', t')$  defined as follows:

$$\frac{\partial^2 \tilde{G}}{\partial t^2}(\mathbf{r}, t; \mathbf{r}', t') - c^2 \nabla^2 \tilde{G}(\mathbf{r}, t; \mathbf{r}', t') = \delta(\mathbf{r} - \mathbf{r}') \delta(t - t')$$
 (2)

where  $\delta$  is the Dirac delta function; homogeneous initial conditions are assumed,  $\tilde{G}(\mathbf{r},t;\mathbf{r}',t') = \partial \tilde{G}/\partial t(\mathbf{r},t;\mathbf{r}',t') = 0$  for all t > t'. The solution to Eq. (2) is well known [3] and is given to be

$$\tilde{G}(\mathbf{r},t;\mathbf{r}',t') = \frac{G_0}{4\pi c^2} \delta\left(t' - t - \frac{R}{c}\right) \tag{3}$$

where  $R(\mathbf{r},\mathbf{r}')=|\mathbf{r}-\mathbf{r}'|$  and  $G_0=1/R(\mathbf{r},\mathbf{r}')$ . The resulting TD-BIE is [5]

$$C_{s}p(\mathbf{r}',t') = \int_{S} \left[ G_{0}(\mathbf{r}_{s},\mathbf{r}') \frac{\partial p}{\partial n}(\mathbf{r}_{s},t'_{R}) - \frac{\partial G_{0}}{\partial n}(\mathbf{r}_{s},\mathbf{r}')(p(\mathbf{r}_{s},t'_{R})) + \frac{R}{c} \frac{\partial p}{\partial t}(\mathbf{r}_{s},t'_{R}) \right] d\mathbf{r}_{s} + \frac{1}{c^{2}} \int_{V} G_{0}(\mathbf{r}_{s},\mathbf{r}')q(\mathbf{r}_{s},t'_{R}) d\mathbf{r}_{s}$$

$$(4)$$

where  $C_s = 4\pi$  when  $\mathbf{r}'$  is an off-surface observer point, and  $C_s = 2\pi$  when  $\mathbf{r}' = \mathbf{r}'_s$  is a smooth point on surface S. Further, V denotes the region of the acoustic source, and  $t'_R = t' - R/c$  is a retarded time value.

Equation (4) is an integral equation for  $p(\mathbf{r}'_s, t')$  that is related to the direct contribution of the source noise q as well as the surface contribution involving the retarded values of p and its normal derivative  $\partial p/\partial n$ . When the pressure and its normal derivatives are calculated on the surface S, Eq. (4) also predicts the pressure at an arbitrary observer point  $\mathbf{r}'$  exterior to the surface. In this paper, surface normal direction is defined to be the one that points into the scattering body.

Time-domain boundary integral equations, such as Eq. (4), have an intrinsic numerical instability [5,6,8,9,18,19] due to the existence of nontrivial solutions in the interior domain at resonant frequencies. Resonant frequencies can be eliminated by using a Burton/Miller-type reformulation of Eq. (4) [5,7–9]. To deal with the impedance boundary condition, unlike the derivation in Ref. [5], both p and  $\partial p/\partial n$  will be included in the derivation process. The Burton–Miller reformulation results by taking the derivative of Eq. (4) at surface points  $\mathbf{r}_s^{\prime}$  in the form of

$$a\frac{\partial}{\partial t'} + bc\frac{\partial}{\partial n'} \tag{5}$$

that is, a linear combination of time and normal derivatives, where a and b are arbitrary parameters that must satisfy the stability condition, a/b < 0, a simple choice being that a = 1 and b = -1 [5,8,9]. Here, t' is the observer time, and  $\partial/\partial n'$  is the normal derivative at the surface observer point  $\mathbf{r}'_s$  as given in Eq. (4).

The scattering surface S is decomposed into rigid and soft surfaces,  $S_0$  and  $S_I$ , respectively, such that  $S = S_0 \cup S_I$ . On rigid surfaces, a solid wall boundary condition is imposed,  $\partial p/\partial n = 0$ . On soft surfaces, an impedance boundary condition is imposed, herein represented by the multipole impedance model and further discussed in Sec. III. Applying Eq. (5) to Eq. (4) and the solid wall boundary condition only on rigid surfaces  $S_0$ , and taking the limit as  $\mathbf{r}' \to \mathbf{r}'_s$ , yields

$$a \left[ 2\pi \frac{\partial p}{\partial t}(\mathbf{r}'_{s}, t') - \int_{S_{l}} G_{0}(\mathbf{r}_{s}, \mathbf{r}'_{s}) \frac{\partial}{\partial t} \left( \frac{\partial p}{\partial n}(\mathbf{r}_{s}, t'_{R}) \right) d\mathbf{r}_{s} \right]$$

$$+ \int_{S} \frac{\partial G_{0}}{\partial n}(\mathbf{r}_{s}, \mathbf{r}'_{s}) \left( \frac{\partial p}{\partial t}(\mathbf{r}_{s}, t'_{R}) + \frac{R}{c} \frac{\partial p}{\partial t^{2}}(\mathbf{r}_{s}, t'_{R}) \right) d\mathbf{r}_{s}$$

$$+ bc \left[ 4\pi \frac{\partial p}{\partial n'}(\mathbf{r}', t') - \frac{\partial}{\partial n'} \int_{S_{l}} G_{0}(\mathbf{r}_{s}, \mathbf{r}') \frac{\partial p}{\partial n}(\mathbf{r}_{s}, t'_{R}) d\mathbf{r}_{s} \right]$$

$$+ \frac{\partial}{\partial n'} \int_{S} \frac{\partial G_{0}}{\partial n}(\mathbf{r}_{s}, \mathbf{r}') (p(\mathbf{r}_{s}, t'_{R}) + \frac{R}{c} \frac{\partial p}{\partial t}(\mathbf{r}_{s}, t'_{R})) d\mathbf{r}_{s}$$

$$= a \frac{\partial Q}{\partial t'}(\mathbf{r}'_{s}, t') + bc \frac{\partial Q}{\partial n'}(\mathbf{r}'_{s}, t')$$

$$(6)$$

where

$$Q(\mathbf{r}_s', t') = \frac{1}{c^2} \int_V G_0(\mathbf{r}_s, \mathbf{r}') q(\mathbf{r}_s, t_R') \, d\mathbf{r}_s \tag{7}$$

Note that the pressure normal derivative term appears only in the integrals over lined surfaces  $S_l$ . Because of the normal derivative operation in the Burton–Miller reformulation, the order of integral singularity is increased compared to Eq. (4). The limit for the integral on the full surface S in the second bracketed term on the left-hand side of Eq. (6) can be simplified as in Ref. [5] [Eq. (33) therein]. The limit for the integral on soft surfaces  $S_l$  involving  $\partial p/\partial n$  can be simplified by first noting that

$$\frac{\partial}{\partial n'} \left( \frac{\partial p}{\partial n} (\mathbf{r}_s, t_R') \right) = \frac{\partial}{\partial t} \left( \frac{\partial p}{\partial n} (\mathbf{r}_s, t_R') \right) \frac{\partial t_R'}{\partial n'}$$

$$\frac{\partial}{\partial n'} \int_{S_l} G_0(\mathbf{r}_s, \mathbf{r}') \frac{\partial p}{\partial n} (\mathbf{r}_s, t_R') \, d\mathbf{r}_s = \int_{S_l} \frac{\partial G_0}{\partial n'} (\mathbf{r}_s, \mathbf{r}') \frac{\partial p}{\partial n} (\mathbf{r}_s, t_R') \, d\mathbf{r}_s$$

$$+ \int_{S_s} G_0(\mathbf{r}_s, \mathbf{r}') \frac{\partial}{\partial t} \left( \frac{\partial p}{\partial n} (\mathbf{r}_s, t_R') \right) \frac{\partial t_R'}{\partial n'} \, d\mathbf{r}_s \tag{8}$$

Noting that the first integral in Eq. (8) involving  $\partial G_0/\partial n'$  is singular, its limit as  $r' \to r'_s$  can be found as follows:

$$\lim_{\mathbf{r}' \to \mathbf{r}'_{s}} \int_{S_{l}} \frac{\partial G_{0}}{\partial n'}(\mathbf{r}_{s}, \mathbf{r}') \frac{\partial p}{\partial n}(\mathbf{r}_{s}, t'_{R}) \, d\mathbf{r}_{s} = \lim_{\mathbf{r}' \to \mathbf{r}'_{s}} \int_{S_{l}} \left[ \frac{\partial G_{0}}{\partial n'}(\mathbf{r}_{s}, \mathbf{r}') + \frac{\partial G_{0}}{\partial n}(\mathbf{r}_{s}, \mathbf{r}') \right] \frac{\partial p}{\partial n}(\mathbf{r}_{s}, t'_{R}) \, d\mathbf{r}_{s} - \lim_{\mathbf{r}' \to \mathbf{r}'_{s}} \int_{S_{l}} \frac{\partial G_{0}}{\partial n}(\mathbf{r}_{s}, \mathbf{r}') \frac{\partial p}{\partial n}(\mathbf{r}_{s}, t'_{R}) \, d\mathbf{r}_{s}$$

$$(9)$$

Further note that, for the first integral presented earlier

$$\frac{\partial G_0}{\partial n'}(\mathbf{r}_s, \mathbf{r}') + \frac{\partial G_0}{\partial n}(\mathbf{r}_s, \mathbf{r}') = \mathbf{n}' \cdot \nabla' G_0 + \mathbf{n} \cdot \nabla G_0$$
$$= -(\mathbf{n}' - \mathbf{n}) \cdot \nabla G_0$$

having used the fact that  $\nabla G_0 = -(\mathbf{r} - \mathbf{r}')/R^3$  and  $\nabla' G_0 = -(\mathbf{r}' - \mathbf{r})/R^3 = -\nabla G_0$ . With a weakened singularity, the first integral in the right-hand side of Eq. (9) is continuous, that is, the limit and integration can be interchanged:

$$\lim_{r' \to r'_s} \int_{S_t} \left[ \frac{\partial G_0}{\partial n'}(\boldsymbol{r}_s, \boldsymbol{r}') + \frac{\partial G_0}{\partial n}(\boldsymbol{r}_s, \boldsymbol{r}') \right] \frac{\partial p}{\partial n}(\boldsymbol{r}_s, t'_R) \, \mathrm{d}\boldsymbol{r}_s$$

$$= \int_{S_t} \left[ \frac{\partial G_0}{\partial n'}(\boldsymbol{r}_s, \boldsymbol{r}'_s) + \frac{\partial G_0}{\partial n}(\boldsymbol{r}_s, \boldsymbol{r}'_s) \right] \frac{\partial p}{\partial n}(\boldsymbol{r}_s, t'_R) \, \mathrm{d}\boldsymbol{r}_s \qquad (10)$$

The second integral in Eq. (9) is the well-known double-layer singular integral, thus giving the following limit [5] [Eq. (18) therein]:

$$\lim_{\mathbf{r}' \to \mathbf{r}'_s} \int_{S_l} \frac{\partial G_0}{\partial n} (\mathbf{r}_s, \mathbf{r}') \frac{\partial p}{\partial n} (\mathbf{r}_s, t'_R) \, d\mathbf{r}_s$$

$$= \int_{S_l} \frac{\partial G_0}{\partial n} (\mathbf{r}_s, \mathbf{r}'_s) \frac{\partial p}{\partial n} (\mathbf{r}_s, t'_R) \, d\mathbf{r}_s - 2\pi \frac{\partial p}{\partial n} (\mathbf{r}'_s, t') \tag{11}$$

Equation (12) follows by combining Eqs. (10) and (11):

$$\lim_{\mathbf{r}' \to \mathbf{r}'_s} \int_{S_l} \frac{\partial G_0}{\partial n'}(\mathbf{r}_s, \mathbf{r}') \frac{\partial p}{\partial n}(\mathbf{r}_s, t'_R) \, d\mathbf{r}_s$$

$$= \int_{S_s} \frac{\partial G_0}{\partial n'}(\mathbf{r}_s, \mathbf{r}'_s) \frac{\partial p}{\partial n}(\mathbf{r}_s, t'_R) \, d\mathbf{r}_s + 2\pi \frac{\partial p}{\partial n}(\mathbf{r}'_s, t')$$
(12)

Hence, by carrying out the limit  $r' \to r'_s$  in Eq. (6) using Eq. (12), the resulting Burton–Miller reformation of Eq. (4) is given in Eq. (13):

$$a \left[ 2\pi \frac{\partial p}{\partial t}(\mathbf{r}'_{s}, t') - \int_{S_{l}} G_{0}(\mathbf{r}_{s}, \mathbf{r}'_{s}) \frac{\partial}{\partial t} \left( \frac{\partial p}{\partial n}(\mathbf{r}_{s}, t'_{R}) \right) d\mathbf{r}_{s} \right]$$

$$+ \int_{S} \frac{\partial G_{0}}{\partial n}(\mathbf{r}_{s}, \mathbf{r}'_{s}) \left( \frac{\partial p}{\partial t}(\mathbf{r}_{s}, t'_{R}) + \frac{R}{c} \frac{\partial p}{\partial t^{2}}(\mathbf{r}_{s}, t'_{R}) \right) d\mathbf{r}_{s} \right]$$

$$+ bc \left[ 2\pi \frac{\partial p}{\partial n}(\mathbf{r}'_{s}, t') - \int_{S_{l}} \frac{\partial G_{0}}{\partial n'}(\mathbf{r}_{s}, \mathbf{r}'_{s}) \left( \frac{\partial p}{\partial n}(\mathbf{r}_{s}, t'_{R}) \right) + \frac{R}{c} \frac{\partial}{\partial t} \left( \frac{\partial p}{\partial n}(\mathbf{r}_{s}, t'_{R}) \right) \right) d\mathbf{r}_{s} \right]$$

$$+ bc \left[ \int_{S} \frac{\partial^{2} G_{0}}{\partial n' \partial n}(\mathbf{r}_{s}, \mathbf{r}'_{s}) \left( p(\mathbf{r}_{s}, t'_{R}) - p(\mathbf{r}'_{s}, t') + \frac{R}{c} \frac{\partial p}{\partial t}(\mathbf{r}_{s}, t'_{R}) \right) d\mathbf{r}_{s} \right]$$

$$- \frac{b}{c} \int_{S} R^{3} \frac{\partial G_{0}}{\partial n'} \frac{\partial G_{0}}{\partial n} \frac{\partial^{2} p}{\partial t^{2}}(\mathbf{r}_{s}, t'_{R}) d\mathbf{r}_{s} = a \frac{\partial Q}{\partial t'}(\mathbf{r}'_{s}, t') + bc \frac{\partial Q}{\partial n'}(\mathbf{r}'_{s}, t')$$

$$(13)$$

Note that, as expected, Eq. (13) reduces to the TD-BIE given in Ref. [5] for rigid-body scattering when the terms involving  $\partial p/\partial n$  are set to be zero. On the surfaces where an acoustic liner is applied, p and  $\partial p/\partial n$  are related through the impedance condition, as described in the next section.

## III. Time-Domain Broadband Impedance Boundary Condition

The impedance boundary condition to be imposed on soft surfaces is defined in the frequency domain as follows:

$$\frac{\hat{p}(\mathbf{r}_s, \omega)}{\hat{v}(\mathbf{r}_s, \omega)} = Z(\omega) \tag{14}$$

where  $Z(\omega)$  is the impedance,  $\hat{p}(r_s, \omega)$  is the acoustic pressure

$$\hat{v}(\mathbf{r}_s,\omega) = \frac{1}{i\omega\rho_0} \frac{\partial \hat{p}}{\partial n}(\mathbf{r}_s,\omega)$$

is the acoustic velocity, and  $\rho_0$  is a constant for the average fluid density. Here, a caret  $\hat{\cdot}$  denotes the frequency-domain variables, assuming a time dependence of  $e^{-i\omega t}$ , in which i is the imaginary unit  $(i^2=-1)$ . In this work, impedance  $Z(\omega)$  is modeled after the multipole impedance model introduced in Refs. [12,14,15]:

$$Z(\omega) = -i\omega h_0 + R_0 + \sum_{\ell=1}^{J_1} \frac{A_{\ell}}{\gamma_{\ell} - i\omega} + \frac{1}{2} \sum_{\ell=1}^{J_2} \left[ \frac{B_{\ell} + iC_{\ell}}{\alpha_{\ell} + i\beta_{\ell} - i\omega} + \frac{B_{\ell} - iC_{\ell}}{\alpha_{\ell} - i\beta_{\ell} - i\omega} \right]$$
(15)

where  $J_1$  is the number of simple poles at  $\omega = -i\gamma_\ell$ ,  $J_2$  is the number of paired poles at  $\omega = -i\alpha_\ell \pm \beta_\ell$ , and  $h_0$  and  $R_0$  are real coefficients. Causality, passivity, and stability lead to  $h_0$ ,  $R_0 \ge 0$ ,  $\gamma_\ell \ge 0$  for

 $\ell = 1, \ldots, J_1$ , and  $\alpha_{\ell} \ge 0$  for  $\ell = 1, \ldots, J_2$ . Causality further requires that  $Z(\omega)$  is both analytical and nonzero, while  $\operatorname{Im}(\omega) > 0$  [17]. Combining Eqs. (14) and (15), and simplifying, yields Eq. (16):

$$i\omega\rho_{0}\hat{p}(\mathbf{r}_{s},\omega) = -i\omega h_{0}\frac{\partial\hat{p}}{\partial n}(\mathbf{r}_{s},\omega) + R_{0}\frac{\partial\hat{p}}{\partial n}(\mathbf{r}_{s},\omega)$$

$$+ \sum_{\ell=1}^{J_{1}} A_{\ell} \left[ \frac{1}{\gamma_{\ell} - i\omega} \frac{\partial\hat{p}}{\partial n}(\mathbf{r}_{s},\omega) \right]$$

$$+ \sum_{\ell=1}^{J_{2}} B_{\ell} \left[ \frac{\alpha_{\ell} - i\omega}{(\alpha_{\ell} - i\omega)^{2} + \beta_{\ell}^{2}} \frac{\partial\hat{p}}{\partial n}(\mathbf{r}_{s},\omega) \right]$$

$$+ \sum_{\ell=1}^{J_{2}} C_{\ell} \left[ \frac{\beta_{\ell}}{(\alpha_{\ell} - i\omega)^{2} + \beta_{\ell}^{2}} \frac{\partial\hat{p}}{\partial n}(\mathbf{r}_{s},\omega) \right]$$
(16)

To facilitate the conversion of Eq. (16) from the frequency domain to the time domain, as in Ref. [14], the following auxiliary variables are defined:

$$\hat{p}_{\ell}^{(0)}(\mathbf{r}_{s},\omega) = \frac{1}{\gamma_{\ell} - i\omega} \frac{\partial \hat{p}}{\partial n}(\mathbf{r}_{s},\omega) \quad \text{for } \ell = 1,\dots,J_{1}$$
 (17)

$$\hat{p}_{\ell}^{(1)}(\mathbf{r}_{s},\omega) = \frac{\alpha_{\ell} - i\omega}{(\alpha_{\ell} - i\omega)^{2} + \beta_{\ell}^{2}} \frac{\partial \hat{p}}{\partial n}(\mathbf{r}_{s},\omega),$$

$$\hat{p}_{\ell}^{(2)}(\mathbf{r}_{s},\omega) = \frac{\beta_{\ell}}{(\alpha_{\ell} - i\omega)^{2} + \beta_{\ell}^{2}} \frac{\partial \hat{p}}{\partial n}(\mathbf{r}_{s},\omega) \quad \text{for } \ell = 1,\dots,J_{2}$$
(18)

such that  $\hat{p}_{\ell}^{(0,1,2)}(\boldsymbol{r}_s,\omega)$  is the Fourier transform of  $p_{\ell}^{(0,1,2)}(\boldsymbol{r}_s,t)$ . Substituting Eqs. (17) and (18) into Eq. (16), and simplifying, yields the following frequency-domain broadband impedance relationship between pressure  $\hat{p}$  and its normal derivative  $\partial \hat{p}/\partial n$ :

$$i\omega\rho_{0}\hat{p}(\mathbf{r}_{s},\omega) = -i\omega h_{0}\frac{\partial\hat{p}}{\partial n}(\mathbf{r}_{s},\omega) + R_{0}\frac{\partial\hat{p}}{\partial n}(\mathbf{r}_{s},\omega) + \sum_{\ell=1}^{J_{1}} A_{\ell}\hat{p}_{\ell}^{(0)}(\mathbf{r}_{s},\omega) + \sum_{\ell=1}^{J_{2}} B_{\ell}\hat{p}_{\ell}^{(1)}(\mathbf{r}_{s},\omega) + \sum_{s=1}^{J_{2}} C_{\ell}\hat{p}_{\ell}^{(2)}(\mathbf{r}_{s},\omega)$$

$$(19)$$

Taking the inverse Fourier transform of Eq. (19) yields the time-domain impedance boundary condition:

$$\rho_0 \frac{\partial p}{\partial t}(\mathbf{r}_s, t) + h_0 \frac{\partial}{\partial t} \left( \frac{\partial p}{\partial n}(\mathbf{r}_s, t) \right) + R_0 \frac{\partial p}{\partial n}(\mathbf{r}_s, t) + \sum_{\ell=1}^{J_1} A_{\ell} p_{\ell}^{(0)}(\mathbf{r}_s, t)$$

$$+ \sum_{\ell=1}^{J_2} B_{\ell} p_{\ell}^{(1)}(\mathbf{r}_s, t) + \sum_{\ell=1}^{J_2} C_{\ell} p_{\ell}^{(2)}(\mathbf{r}_s, t) = 0$$
(20)

Manipulating and taking the inverse Fourier transforms of Eqs. (17) and (18) yield Eq. (21), for  $\ell = 1, \ldots, J_1$ :

$$\frac{\partial p_{\ell}^{(0)}}{\partial t}(\boldsymbol{r}_{s},t) + \gamma_{\ell} p_{\ell}^{(0)}(\boldsymbol{r}_{s},t) = \frac{\partial p}{\partial n}(\boldsymbol{r}_{s},t)$$
(21)

and Eq. (22), for  $\ell = 1, ..., J_2$ 

$$\frac{\partial p_{\ell}^{(1)}}{\partial t}(\mathbf{r}_{s},t) + \alpha_{\ell} p_{\ell}^{(1)}(\mathbf{r}_{s},t) + \beta_{\ell} p_{\ell}^{(2)}(\mathbf{r}_{s},t) = \frac{\partial p}{\partial n}(\mathbf{r}_{s},t),$$

$$\frac{\partial p_{\ell}^{(2)}}{\partial t}(\mathbf{r}_{s},t) - \beta_{\ell} p_{\ell}^{(1)}(\mathbf{r}_{s},t) + \alpha_{\ell} p_{\ell}^{(2)}(\mathbf{r}_{s},t) = 0$$
(22)

Equations (20–22) are the constitutive forms of the time-domain broadband impedance boundary condition.

#### IV. Numerical Discretization

In this section, the discretization of the TD-BIE, Eq. (13), coupled with the time-domain broadband multipole impedance boundary condition, Eqs. (20–22), by the time-domain boundary element method is described. Let the surface S be divided into a set of  $N_e$  boundary elements  $\{E_j, j = 1, \ldots, N_e\}$ , where the collocation point  $r_j$  is located at the centroid of element  $E_j$ . The time domain is divided into  $N_t$  uniform time steps, where  $t_k = k\Delta t$ ,  $k = 1, \ldots, N_e$ .

All terms  $p(\mathbf{r}_s, t)$  and  $\partial p/\partial n(\mathbf{r}_s, t)$  are approximated by using surface-element basis functions  $\phi_j(\mathbf{r}_s)$  and temporal basis functions  $\psi_k(t)$  as follows:

$$p(\mathbf{r}_s, t) = \sum_{k=0}^{N_t} \sum_{j=1}^{N_e} u_j^k \phi_j(\mathbf{r}_s) \psi_k(t) \quad \text{and}$$

$$\frac{\partial p}{\partial n}(\mathbf{r}_s, t) = \sum_{k=0}^{N_t} \sum_{j=1}^{N_e} v_j^k \phi_j(\mathbf{r}_s) \psi_k(t) \tag{23}$$

In Eq. (23),  $u_j^k$  and  $v_j^k$  denote the values of the solution of  $p(\boldsymbol{r}_s,t)$  and  $\partial p/\partial n(\boldsymbol{r}_s,t)$ , respectively, of the jth node at time  $t_k$ . On any rigid element, it is assumed that  $v_j^k = 0$  as a result of the solid wall boundary condition [i.e.,  $\partial p/\partial n(\boldsymbol{r}_s,t) = 0$ ] on rigid surfaces  $S_0$ . In the spatial domain, zeroth-order basis functions are considered,  $\phi_j(\boldsymbol{r}_s) = 1$ , if  $\boldsymbol{r}_s$  is on element  $E_j$  containing node  $\boldsymbol{r}_j$  and  $\phi_j(\boldsymbol{r}_s) = 0$  otherwise. In the temporal domain, the third-order Lagrange basis functions are considered:

$$\Psi(\tau) = \begin{cases}
1 + \frac{11}{6}\tau + \tau^2 + \frac{1}{6}\tau^3, & -1 < \tau \le 0 \\
1 + \frac{1}{2}\tau - \tau^2 - \frac{1}{2}\tau^3, & 0 < \tau \le 1 \\
1 - \frac{1}{2}\tau - \tau^2 + \frac{1}{2}\tau^3, & 1 < \tau \le 2 \\
1 - \frac{11}{6}\tau + \tau^2 - \frac{1}{6}\tau^3, & 2 < \tau \le 3 \\
0, & \text{other}
\end{cases} \tag{24}$$

such that  $\psi_k(t) = \Psi((t - t_k)/\Delta t)$ . All surface integrations are computed by high-order Gauss quadrature on a  $6 \times 6$  grid for each element.

By evaluating the discretized Burton–Miller reformulation at collocation points  $\mathbf{r}_j$  on the center of elements  $E_j$ ,  $j=1,\ldots,N_e$  and at time step  $t_n$  using basis functions  $\phi_j(\mathbf{r}_s)$  and  $\psi_k(t)$ , Eq. (13) is cast into a system of equations of the form:

$$B_0 u^n + C_0 v^n = q^n - B_1 u^{n-1} - C_1 v^{n-1} - B_2 u^{n-2} - C_2 v^{n-2} - \dots - B_J u^{n-J} - C_J v^{n-J}$$
(25)

where  $u^k$  and  $v^k$  denote the vector that contains all unknowns  $\{u^k_j, j=1, \ldots, N_e\}$  and  $\{v^k_j, j=1, \ldots, N_e\}$ , respectively, at time level  $t_k$ . Because of the limited temporal stencil width of Eq. (24), the B and C matrices are sparse. Additionally, the index J denotes the maximum time history of the solution required for Eq. (25) and is dependent on the dimensions of the scattering surface [5].

Equation (25) is a march-on-in-time scheme, in which a sparse matrix is solved iteratively using retarded time values for the right-hand side. For rigid-body scattering only, all terms  $v^k$  in Eq. (25) are equivalently zero and a solution can be obtained for  $u^k$ . With soft surfaces, a second system is needed to couple with Eq. (25) for obtaining solutions of both  $u^k$  and  $v^k$ . This system results by direct application of the impedance boundary condition defined in Eqs. (20–22) as detailed next.

The constitutive form of the time-domain broadband impedance boundary condition, Eqs. (20–22), is discretized by approximating  $p_{\ell}^{(m)}(\mathbf{r}_s,t)$ , m=0,1,2, using the same surface-element basis functions  $\phi_j(\mathbf{r}_s)$  and temporal basis functions  $\psi_k(t)$  as in Eqs. (23) and (24):

$$p_{\ell}^{(m)}(\mathbf{r}_{s},t) = \sum_{k=0}^{N_{t}} \sum_{j=1}^{N_{e}} \left( p_{\ell}^{(m)} \right)_{j}^{k} \phi_{j}(\mathbf{r}_{s}) \psi_{k}(t), \qquad m = 0, 1, 2 \quad (26)$$

where  $(p_{\ell}^{(m)})_j^k$  denotes the value of  $p_{\ell}^{(m)}(\mathbf{r}_s, t)$  at the *j*th node and time  $t_k$ . Substituting Eq. (26) into Eqs. (20–22) and evaluating at collocation points  $\mathbf{r}_j$ ,  $j = 1, \dots, N_e$  and time step  $t_n$ , and simplifying by the temporal basis function given in Eq. (24), yield the following discretized broadband impedance boundary condition:

$$\sum_{k=0}^{3} \left[ u_{j}^{n-k} \rho_{0} \psi_{n-k}'(t_{n}) + v_{j}^{n-k} (h_{0} \psi_{n-k}'(t_{n}) + R_{0} \psi_{n-k}(t_{n})) \right]$$

$$+ \sum_{\ell=1}^{J_{1}} (p_{\ell}^{(0)})_{j}^{n} A_{\ell} + \sum_{\ell=1}^{J_{2}} (p_{\ell}^{(1)})_{j}^{n} B_{\ell} + \sum_{\ell=1}^{J_{2}} (p_{\ell}^{(2)})_{j}^{n} C_{\ell} = 0$$

$$(27)$$

$$\sum_{k=0}^{3} \left( p_{\ell}^{(0)} \right)_{j}^{n-k} [\psi_{n-k}'(t_{n}) + \gamma_{\ell} \psi_{n-k}(t_{n})] = v^{n}, \qquad \ell = 1, \dots, J_{1}$$
(28)

$$\sum_{k=0}^{3} (p_{\ell}^{(1)})_{j}^{n-k} [\psi_{n-k}'(t_{n}) + \alpha_{\ell} \psi_{n-k}(t_{n})] + \beta_{\ell} (p_{\ell}^{(2)})_{j}^{n} = v^{n},$$

$$\ell = 1, \dots, J_{2}$$
(29)

$$-\sum_{k=0}^{3} (p_{\ell}^{(2)})_{j}^{n-k} [\psi_{n-k}'(t_{n}) + \alpha_{\ell} \psi_{n-k}(t_{n})] + \beta_{\ell} (p_{\ell}^{(1)})_{j}^{n} = 0,$$

$$\ell = 1, \dots, J_{2}$$
(30)

for  $j = 1, ..., N_e$ , where a prime denotes derivative. This is equivalent to the results of discretizing Eqs. (20–22) by the third-order implicit backward difference scheme [20].

third-order implicit backward difference scheme [20]. Denoting  $p_{\ell}^{(0)}$ ,  $\ell=1,\ldots,J_1$ , and  $p_{\ell}^{(1,2)}$ ,  $\ell=1,\ldots,J_2$ , as the vectors that contain the auxiliary variables from all points where the impedance boundary condition is applied, the following vectors are additionally defined by Eq. (31):

$$\mathbf{P}_{(0)} = \begin{bmatrix} \mathbf{p}_{1}^{(0)} \mathbf{p}_{2}^{(0)} & \cdots & \mathbf{p}_{J_{1}}^{(0)} \end{bmatrix}^{T}, \qquad \mathbf{P}_{(1)} = \begin{bmatrix} \mathbf{p}_{1}^{(1)} \mathbf{p}_{2}^{(1)} & \cdots & \mathbf{p}_{J_{2}}^{(1)} \end{bmatrix}^{T}, \quad \text{and} \\
\mathbf{P}_{(2)} = \begin{bmatrix} \mathbf{p}_{1}^{(2)} \mathbf{p}_{2}^{(2)} & \cdots & \mathbf{p}_{J_{2}}^{(2)} \end{bmatrix}^{T} \tag{31}$$

Using Eq. (31), along with  $u^k$  and  $v^k$ , the discretized solutions of Eqs. (27–30) can be expressed succinctly as the following system of equations:

$$D_{0}u^{n} + E_{0}v^{n} + F_{0}P_{(0)}^{n} + G_{0}P_{(1)}^{n} + H_{0}P_{(2)}^{n}$$

$$= -\sum_{k=1}^{3} [D_{k}u^{n-k} + E_{k}v^{n-k}]$$
(32)

$$\mathcal{J}_0 \mathbf{v}^n + \mathcal{K}_0 \mathbf{P}_{(0)}^n = -\sum_{k=1}^3 [\mathcal{K}_k \mathbf{P}_{(0)}^{n-k}]$$
 (33)

$$\mathcal{L}_{0}v^{n} + \mathcal{M}_{0}P_{(1)}^{n} + \mathcal{N}_{0}P_{(2)}^{n} = -\sum_{k=1}^{3} [\mathcal{M}_{k}P_{(1)}^{n-k}]$$
 (34)

$$\mathcal{P}_0 P_{(1)}^n + \mathcal{Q}_0 P_{(2)}^n = -\sum_{k=1}^3 [\mathcal{Q}_k P_{(2)}^{n-k}]$$
 (35)

The nonzero entries of Eqs. (32–35) are given by

$$\begin{split} & \boldsymbol{D}_{k} = \rho_{0} \boldsymbol{\psi}_{n-k}^{\prime}(t_{n}) \boldsymbol{I}_{N_{e} \times N_{e}}, \\ & \boldsymbol{E}_{k} = (h_{0} \boldsymbol{\psi}_{n-k}^{\prime}(t_{n}) + R_{0} \boldsymbol{\psi}_{n-k}(t_{n})) \boldsymbol{I}_{N_{e} \times N_{e}}, \quad k = 0, 1, 2, 3 \\ & \boldsymbol{F}_{0} = [A_{1} \boldsymbol{I}_{N_{e} \times N_{e}} \cdots A_{J_{1}} \boldsymbol{I}_{N_{e} \times N_{e}}]_{N_{e} \times J_{1} N_{e}}, \\ & \boldsymbol{G}_{0} = [B_{1} \boldsymbol{I}_{N_{e} \times N_{e}} \cdots B_{J_{2}} \boldsymbol{I}_{N_{e} \times N_{e}}]_{N_{e} \times J_{2} N_{e}} \\ & \boldsymbol{H}_{0} = [C_{1} \boldsymbol{I}_{N_{e} \times N_{e}} \cdots C_{J_{2}} \boldsymbol{I}_{N_{e} \times N_{e}}]_{N_{e} \times J_{2} N_{e}} \\ & \boldsymbol{\mathcal{I}}_{N_{e} \times N_{e}} \\ & \vdots \\ & \boldsymbol{\mathcal{I}}_{N_{e} \times N_{e}} \end{bmatrix}_{J_{1} N_{e} \times N_{e}} & \boldsymbol{\mathcal{I}}_{N_{e} \times N_{e}} \\ & \boldsymbol{\mathcal{I}}_{N_{e} \times N_{e}} \end{bmatrix}_{J_{2} N_{e} \times N_{e}} \\ & \boldsymbol{\mathcal{P}}_{0} = -\boldsymbol{\mathcal{N}}_{0} = \begin{bmatrix} \boldsymbol{\beta}_{1} \boldsymbol{\mathcal{I}}_{N_{e} \times N_{e}} \\ & \vdots \\ & \boldsymbol{\beta}_{J_{2}} \boldsymbol{\mathcal{I}}_{N_{e} \times N_{e}} \end{bmatrix}_{J_{2} N_{e} \times J_{2} N_{e}} \\ & \boldsymbol{\mathcal{K}}_{k} = \begin{bmatrix} \boldsymbol{\eta}_{k}^{1} \boldsymbol{\mathcal{I}}_{N_{e} \times N_{e}} \\ & \vdots \\ & \boldsymbol{\eta}_{k}^{J_{1}} \boldsymbol{\mathcal{I}}_{N_{e} \times N_{e}} \end{bmatrix}_{J_{1} N_{e} \times J_{1} N_{e}} \\ & \text{ere } \boldsymbol{\eta}_{k}^{\ell} = -(\boldsymbol{\psi}_{n-k}^{\prime}(t_{n}) + \boldsymbol{\gamma}_{\ell} \boldsymbol{\psi}_{n-k}(t_{n})), \quad k = 0, 1, 2, 3 \\ & \boldsymbol{\mathcal{M}}_{k} = \boldsymbol{\mathcal{Q}}_{k} = \begin{bmatrix} \boldsymbol{\mu}_{k}^{1} \boldsymbol{\mathcal{I}}_{N_{e} \times N_{e}} \\ & \vdots \\ & \boldsymbol{\mu}_{k}^{J_{2}} \boldsymbol{\mathcal{I}}_{N_{e} \times N_{e}} \end{bmatrix}_{J_{2} N_{e} \times J_{2} N_{e}} \end{aligned}$$

where  $I_{N_e \times N_e}$  is the identity matrix of size  $N_e \times N_e$ .

Coupling Eqs. (32–35) with Eq. (25) allows for the application of the broadband impedance boundary condition, modeled by Eq. (15). This coupled system has a dimension up to  $N_e(2 + J_1 +$  $2J_2$ ) ×  $N_e(2 + J_1 + 2J_2)$  when the impedance boundary condition is applied to all surface elements. When solved iteratively, it provides solutions for  $u^k$  and  $v^k$  on all soft surfaces.

## V. Numerical Eigenvalue Study and Stability Analysis

The solution of the coupled march-on-in-time scheme, Eqs. (25) and (32–35), provides the acoustic scattering by a body with lined surfaces from a given noise source. Examples of numerical solutions will be presented in Sec. VI. To assess the stability for this coupled system, a numerical eigenvalue study is conducted. For convenience of discussion, the coupled system of Eqs. (25) and (32–35) is denoted formally by

$$A_0 \mathbf{w}^n = \mathbf{q}_0^n - A_1 \mathbf{w}^{n-1} - A_2 \mathbf{w}^{n-2} - A_3 \mathbf{w}^{n-3} - \dots - A_J \mathbf{w}^{n-J}$$
(36)

where  $\boldsymbol{w}^k$  is a vector that contains  $\boldsymbol{u}^k$ ,  $\boldsymbol{v}^k$ ,  $\boldsymbol{P}_{(0)}^k$ ,  $\boldsymbol{P}_{(1)}^k$ , and  $\boldsymbol{P}_{(2)}^k$  at time step  $t_k$ . For the stability study, eigenvalue analysis is concerned only with the homogeneous system. The homogeneous system is representative of when the source, or incident wave, has traveled far beyond the scattering body, and it is often when numerical instability

Equation (36), without the source term, can be written equivalently as a standard iteration operation:

$$\mathbf{W}^n = \mathbf{A} \mathbf{W}^{n-1} \tag{37}$$

$$\mathbf{A} = \begin{bmatrix} -\mathbf{A}_0^{-1} \mathbf{A}_1 & -\mathbf{A}_0^{-1} \mathbf{A}_2 & \cdots & -\mathbf{A}_0^{-1} \mathbf{A}_{J-2} & -\mathbf{A}_0^{-1} \mathbf{A}_{J-1} & -\mathbf{A}_0^{-1} \mathbf{A}_J \\ \mathbf{I} & 0 & \cdots & 0 & 0 & 0 \\ 0 & \mathbf{I} & \cdots & 0 & 0 & 0 \\ \vdots & & \ddots & & \vdots & \vdots \\ 0 & 0 & \cdots & \mathbf{I} & 0 & 0 \\ 0 & 0 & \cdots & 0 & \mathbf{I} & 0 \end{bmatrix}$$

and 
$$W^n = \begin{bmatrix} w \\ w^{n-1} \\ w^{n-2} \\ \vdots \\ w^{n-J+2} \\ w^{n-J+1} \end{bmatrix}$$

The matrix power iteration method [21] is then used to find the largest eigenvalue of A in Eq. (37). Herein, the power iteration method proceeds as follows:

- 1) Define an arbitrary unit vector to be  $\boldsymbol{\xi}^{(0)}$ . 2) For  $k=1,2,\ldots$ , calculate  $\boldsymbol{e}^{(k)}=A\boldsymbol{\xi}^{(k-1)}, \boldsymbol{\xi}^{(k)}=\boldsymbol{e}^{(k)}/\|\boldsymbol{e}^{(k)}\|_2$ , and  $\lambda^{(k)}=[\boldsymbol{\xi}^{(k)}]^TA\boldsymbol{\xi}^{(k)}=[\boldsymbol{\xi}^{(k)}]^T\boldsymbol{e}^{(k+1)}$ .
- 3) Calculate the difference between consecutive eigenvalues,  $|\lambda^{(k)} - \lambda^{(k-1)}|$ .
- 4) Repeat until the iterative scheme has converged to the largest eigenvalue,  $|\lambda|_{\text{max}}$  (i.e., when  $|\lambda^{(k)} - \lambda^{(k-1)}|/|\lambda^{(k)}| < \delta$  for a given tolerance  $\delta$ ). In the current study, the tolerance is chosen to be  $\delta = 10^{-9}$ .

The stability of Eq. (36) [i.e., the coupled march-on-in-time system of Eqs. (25) and (32) through (35)] is investigated by considering the scattering by a flat plate with dimension  $[-0.5, 0.5] \times [-0.5, 0.5] \times$ [-0.1, 0.1]. The surface of the flat plate is discretized in the x, y, and z directions with  $N_x$ ,  $N_y$ , and  $N_z$  elements, respectively, giving a total number of  $N_e = 2(N_x N_y + N_y N_z + N_x N_z)$  surface elements. The  $1 (N_e = 70 \text{ elements}), 10 \times 10 \times 2 (N_e = 280 \text{ elements}), 20 \times 20 \times 4$  $(N_e = 1120 \text{ elements})$ , and  $30 \times 30 \times 6$   $(N_e = 2520 \text{ elements})$ . Further, the following two different time steps are considered:  $\Delta t = 1/12$ and  $\Delta t = 1/24$ . This combination of grid size and time step ensures that the scattering problem provides solutions over a wide range of frequencies.

The liner impedance boundary condition is modeled using experimental data. Two acoustic liners, named CT57 and GE03, will be considered. These two liners were tested in the Grazing Flow Impedance Tube at the NASA Langley Research Center Liner Technology Facility. During the tests [22], impedance values were educed over a wide range of frequencies. Using the measured data, broadband multipole impedance models of the form in Eq. (15) were generated using a least-squares regression process. The values for the parameters, which define the surface impedance model in Eq. (15), are shown in Table 1. Because multipole expansion fitting to measured data is not unique, depending on the choices for the number of poles and whether or not to include  $h_0$  and  $R_0$  terms, etc., various possibilities are considered in Table 1.

In each of the liner models shown in Table 1, cases 1 through 4, the parameters yielded Re(Z) > 0, thus preserving passivity. The CT57 liner is depicted in Fig. 1a for cases 1 and 2, colored in black and orange, respectively; the GE03 liner is depicted in Fig. 1b for cases 3 and 4, colored in black and orange, respectively. The experimental data are plotted using markers; resistance, Re(Z), is denoted by circles, and reactance, Im(Z), is denoted by squares. The multipole fitted models are graphed with a dotted line. All values of impedance are nondimensionalized by  $\rho_0 c$ . Frequency is nondimensionalized by c/L, where c = 340 m/s and  $\bar{L} = 1 \text{ m}$ .

For the stability assessment, two configurations of acoustic liner application are considered. First, it is assumed that the acoustic liner

		1401	-	Constants	used for the	010	Touabana impedance model					
				$A_{\ell}$	$\gamma_{\ell}$		$B_{\ell}$	$C_\ell$	$lpha_\ell$	$eta_\ell$		
Case	$h_0$	$R_0$	$J_1$	$\ell=1$ ,	$\dots, J_1$	$J_2$		$\ell=1$ ,	$\dots, J_2$			
1 (CT57)	0.010873	0.177655	1	18.467174	0.985273	2	43.919202 23.611034	-0.571804 -8.511097	4.887694 7.670216	37.631479 -66.460858		
2 (CT57)	0	0.068743	1	18.421975	1.075243	2	99.855347 44.089363	-9.968384 -0.709128	7.952528 4.879110	82.203159 37.451098		
3 (GE03)	0.011775	0.001514	1	32.573728	1.896347	2	0.001101 75.213211	-9.910991 -9.915633	22.599229 7.374808	16.476064 82.791519		
4 (GE03)	0	0	1	32.762971	1.992922	3	100 0.023790 100	-9.866975 -9.993868 -9.905435	9.578137 20.530002 4.032688	93.987180 18.832024 99.876360		

Table 1 Constants used for the broadband impedance model

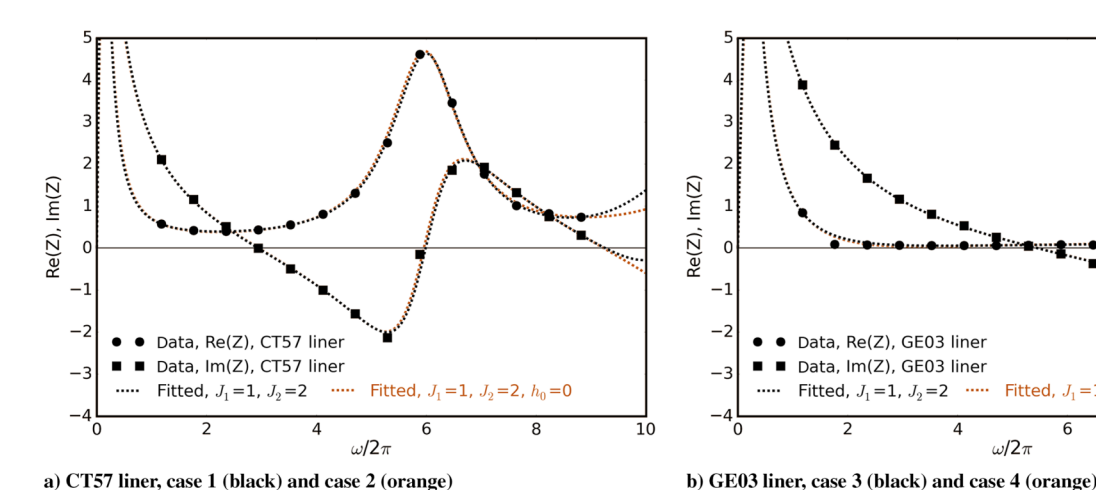


Fig. 1 Illustration of the generated broadband impedance curves using least-squares regression.

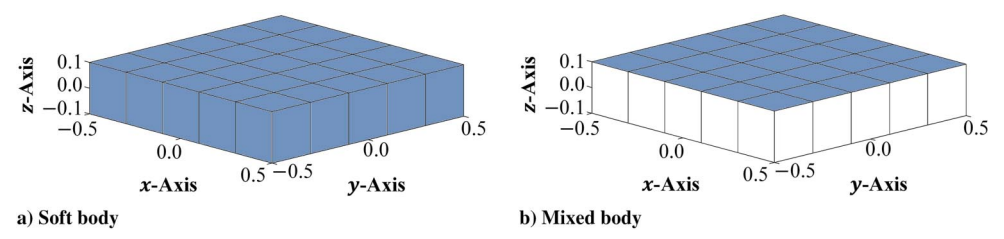


Fig. 2 Comparison between a fully lined and a partially lined scattering body for a flat plate.

is installed on all scattering surfaces, herein referred to as *all-soft*. This configuration is illustrated in Fig. 2a. In the second configuration, it is assumed that the acoustic liner is installed on the top surface of the flat plate, and the rest of the surfaces are treated as solid surfaces, herein referred to as *mixed*. This configuration is illustrated in Fig. 2b. Both all-soft and mixed-body liner applications are assessed for their stability in solving the system. The rigid-body case is used as a baseline, where the stability of the numerical algorithm is tested assuming no liner boundary condition on any scattering

surface. For the baseline assessment, all vectors associated with the liner impedance condition are set equal to zero.

The maximum eigenvalues for both all-soft and mixed bodies are listed in Table 2. Any eigenvalues greater than unity are indicated by **bold** text. The rigid-body results are not listed in the table because, as expected, all baseline cases yield a maximum eigenvalue of unity for all discretizations, time steps, and temporal basis functions confirming that the Burton–Miller reformulation of the TD-BIE provides numerical stability for rigid-body scattering [5].

Table 2 Maximum eigenvalues calculated for the broadband impedance model

Liner	Broadband		$\Delta t =$	= 1/12		$\Delta t = 1/24$				
application	model case no.	$5 \times 5 \times 1$	$10 \times 10 \times 2$	$20 \times 20 \times 4$	30 × 30 × 6	$5 \times 5 \times 1$	$10 \times 10 \times 2$	$20 \times 20 \times 4$	$30 \times 30 \times 6$	
All-soft body	1	1.000000	1.000000	1.000000	1.000000	1.000000	1.000000	1.000000	1.000000	
•	2	1.000000	1.000000	1.000000	1.000000	1.000000	1.000000	1.000000	1.000000	
	3	0.999976	1.000231	1.000116	1.000029	1.000017	0.999965	0.999967	0.999994	
	4	1.000000	1.000000	1.000000	1.000000	1.000000	1.000000	1.000000	1.000000	
Mixed body	1	1.000000	1.000000	1.000000	1.000000	1.000000	1.000000	1.000000	1.000000	
	2	1.000000	1.000000	1.000000	1.000000	1.000000	1.000000	1.000000	1.000000	
	3	1.000148	1.000173	1.000073	1.000027	0.999999	0.999981	0.999991	0.999995	
	4	1.000000	1.000000	1.000000	1.000000	1.000000	1.000000	1.000000	1.000000	

As shown in Table 2, for both all-soft and mixed-body scattering, apart from case 3, all analyses yield a maximum eigenvalue no greater than unity, rendering their stability for the eigenvalues of the iteration matrix A. For case 3, maximum eigenvalues slightly greater than unity are seen but become less than unity as the spatial and temporal resolutions are increased. Note that when the length of elements (assuming a square element)  $\Delta x < 2c\Delta t$ , the matrix  $B_0$  in Eq. (25), which represents the elementwise interactions within the same time step, becomes a banded matrix, leading to an implicit scheme for

e) GE03 liner, case 3, comparisons (sphere)

solving  $u^n$ , where implicitness generally improves numerical stability [23]. These results are consistent with previous work by the authors [24,25].

# VI. Numerical Examples

To demonstrate the validity and stability of the time-domain boundary element method coupled with the broadband multipole impedance boundary condition, numerical examples of scattering by soft surfaces are presented. The following two geometries are considered: a sphere

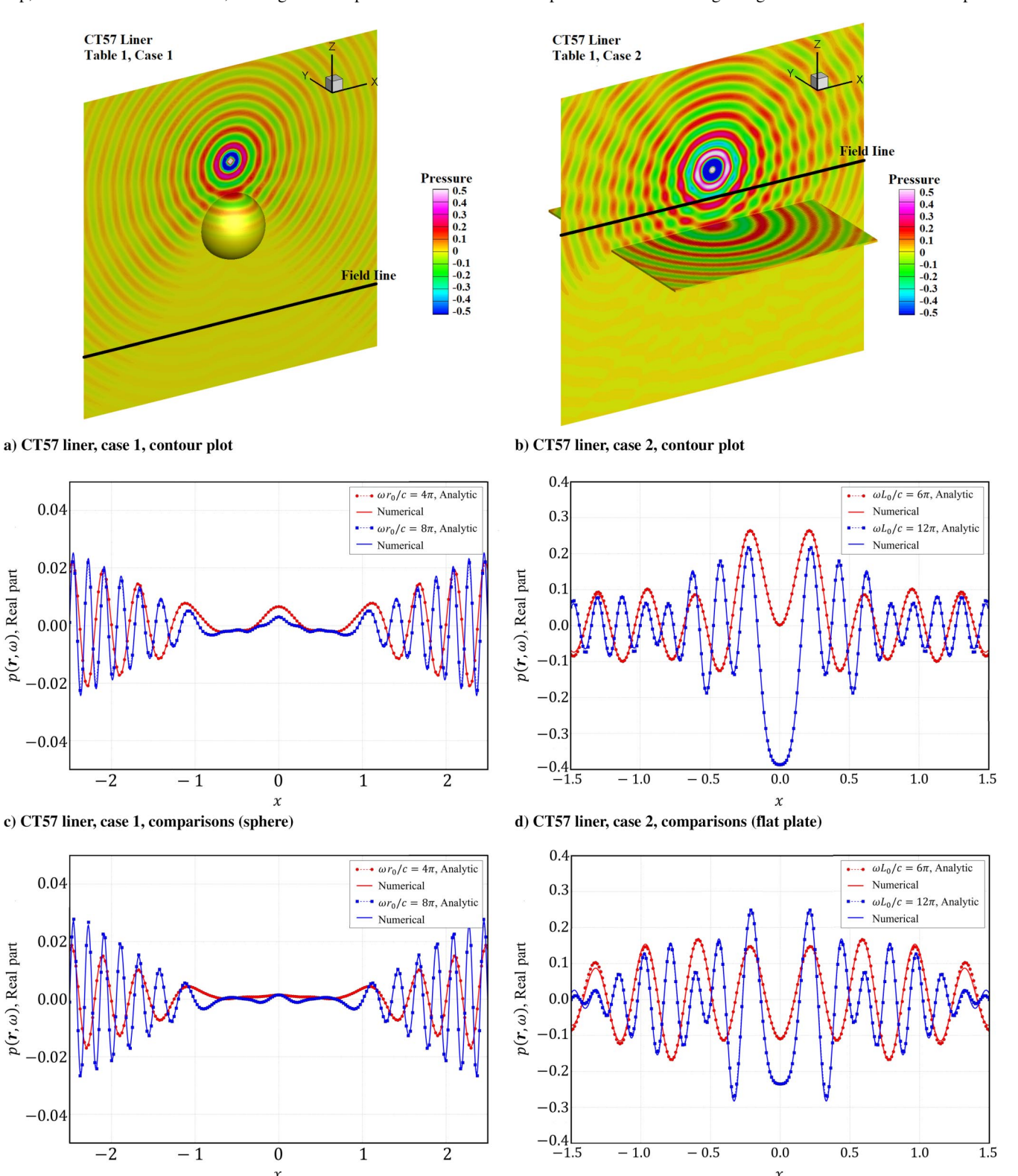


Fig. 3 Numerical examples of scattering by soft surfaces.

f) GE03 liner, case 4, comparisons (flat plate)

and a flat plate. For the sphere, the numerical solution is compared with the known analytical solution (Appendix A). For the flat plate, an analytical solution (Appendix B) of a point-source reflection by an infinite flat surface is used to approximately compare with the computational result.

For the first example, scattering of a point source by a lined sphere of radius  $r_0 = 0.5$ , centered at  $\mathbf{r} = (0,0,0)$ , is considered. The sphere is discretized by a total of  $N_e = 15,360$  quadrilateral elements. A point source is located at  $\mathbf{r}_p = (0,0,1)$ , and the source function as it appears in Eq. (1) is of the form

$$q(\mathbf{r},t) = e^{-\sigma t^2} \delta(\mathbf{r} - \mathbf{r}_p)$$
 (38)

where  $\sigma=1.42/(6\Delta t)^2$ , and  $\Delta t$  is the time step for the time-domain march-on-in-time scheme. For the results shown, the non-dimensional time step is  $c\Delta t/r_0=0.01$ . The march-on-in-time scheme, Eq. (25), coupled with the liner impedance boundary condition, Eqs. (32–35), is solved for the time-domain solution, which is then converted to the frequency domain by the Fourier transform. For a limited number of selected frequencies, as noted in Ref. [5], the frequency-domain solution can be computed concurrently with the time-domain simulation as the following summation:

$$\hat{p}(\mathbf{r},\omega) = \Delta t [p(\mathbf{r},t_1)e^{i\omega t_1} + p(\mathbf{r},t_2)e^{i\omega t_2} + \cdots + p(\mathbf{r},t_{N_t})e^{i\omega t_{N_t}}]$$
(39)

Both the CT57 and GE03 liners discussed in previous sections have been applied for this example, and numerical stability has been observed for the four models shown in Table 1. Figure 3a shows a pressure contour plot of the solution at nondimensional frequency  $\omega r_0/c = 8\pi$  when the CT57 liner impedance boundary condition (Table 1; case 1) is applied on all surface elements of the sphere. Comparisons with the analytical solution along a field line defined by  $-2.5 \le x \le 2.5$ , y = 0, z = -1.5 are shown in Fig. 3c for nondimensional frequencies  $\omega r_0/c = 4\pi$ and  $\omega r_0/c = 8\pi$ , and excellent agreement between the two solutions is observed. The numerical solution for this example, when the GE03 liner (Table 1; case 3) is applied, is shown in Fig. 3e. Again, excellent agreement between the numerical and analytical solutions is observed. The computational run time for this example is approximately 1.5 s per time step on a cluster of eight graphic processing units (GPUs; NVIDIA V100 model) for a total of 4000 time steps (about 1.7 h). The total number of steps is determined so that all scattered waves have essentially exited the computational domain.

In the second example, scattering by a lined flat plate defined by  $[-L_0, L_0] \times [-L_0, L_0] \times [-0.02L_0, 0]$  in the x, y, and z directions, respectively, is considered. Here,  $L_0 = 1$ . The surfaces are discretized by quadrilateral elements with the number of elements per dimension being  $N_x = N_y = 201$ ,  $N_z = 4$ , as described in Sec. V, giving a total of  $N_e = 84{,}018$  elements. As in the first example, the multipole liner impedance boundary condition is applied to all elements on the surface of the plate. A point source of the form Eq. (38) is applied at  $\mathbf{r}_p = (0, 0, 0.5)$ , and a time-domain solution is obtained by solving the march-on-in-time scheme Eq. (25) coupled with Eqs. (32–35). The nondimensional time step is  $c\Delta t/L_0 = 0.005$ , or  $c\Delta t/\Delta x \approx 0.5$ , where  $\Delta x$  is the length of each element for the top and bottom surfaces of the plate. Again, numerical stability is observed for the four models in Table 1. Figure 3b shows the converted frequency-domain solution at nondimensional frequency  $\omega L_0/c = 12\pi$  when the CT57 liner impedance boundary condition (Table 1; case 2) is applied on all surface elements of the plate. The computed solution along a field line defined by  $-1.5 \le x$  $\leq 1.5$ , y = 0, z = 0.25 is compared with the analytical solution of a point-source reflection by an infinite flat surface, given in Appendix B, for nondimensional frequencies  $\omega L_0/c = 6\pi$  and  $\omega L_0/c = 12\pi$ . The comparisons are shown in Figs. 3d and 3f for the solutions by the CT57 and GE03 liner models (Table 1; cases 2 and 4, respectively). The numerical solution agrees very well with the analytical solution, except near the edge of the domain where the numerical solution included the diffraction effects due to the finite extent of the plate in the computation, whereas the analytical solution assumed an infinitely large surface. The computational time for this example is approximately 10.5 h for 4000 time steps on a cluster of eight GPUs.

# VII. Conclusions

The objective of this study was to investigate the feasibility and stability for modeling acoustic wave scattering using a Burton–Miller TD-BIE with impedance boundary condition for the case of no mean flow. Derivation of the TD-BIE with impedance boundary condition, stabilized through a Burton–Miller reformulation, was presented. The impedance boundary condition was implemented using a multipole broadband impedance model. The numerical stability was assessed by an eigenvalue analysis conducted for the coupled march-on-in-time scheme assuming both fully and partially lined bodies. Stability of the coupled system has been observed in numerical simulations. Furthermore, numerical examples with favorable comparisons with known analytical solutions demonstrated the validity of the numerical method presented in this paper.

### Appendix A: Reflection of a Point Source by a Lined Sphere

The analytical solution for the first numerical example of a point-source reflection by a sphere with an impedance boundary condition in the frequency domain is given as follows for completeness [26]. Let the incident wave with point source centered at  $\mathbf{r}_0 = (r_0, \theta_0, \varphi_0)$  be expressed in spherical coordinates as

$$\begin{split} \hat{p}_{\text{inc}} &= \frac{e^{ik|r-r_0|}}{4\pi|r-r_0|} \\ &= \begin{cases} ik \sum_{\ell=0}^{\infty} \sum_{m=-\ell}^{\ell} j_{\ell}(kr_0) h_{\ell}^{(1)}(kr) Y_{\ell m}^*(\theta_0, \varphi_0) Y_{\ell m}(\theta, \varphi) & r > r_0 \\ ik \sum_{\ell=0}^{\infty} \sum_{m=-\ell}^{\ell} j_{\ell}(kr) h_{\ell}^{(1)}(kr_0) Y_{\ell m}^*(\theta_0, \varphi_0) Y_{\ell m}(\theta, \varphi) & r < r_0 \end{cases} \end{split}$$

where  $k = \omega/c$ . Here, the spherical harmonics function is

$$Y_{\ell m}(\theta, \varphi) = \sqrt{\frac{2\ell + 1}{4\pi} \frac{(\ell - m)!}{(\ell + m)!}} P_{\ell}^{m}(\cos \theta) e^{im\varphi}$$

and the spherical Bessel functions are

$$j_{\ell}(x) = \sqrt{\frac{\pi}{2x}} J_{\ell+(1/2)}(x)$$

and

$$h_{\ell}^{(1,2)} = \sqrt{\frac{\pi}{2x}} [J_{\ell+(1/2)}(x) \pm iN_{\ell+(1/2)}(x)]$$

Then, the reflected wave can be expressed as

$$\hat{p}_{\mathrm{ref}} = \sum_{\ell=0}^{\infty} \sum_{m=-\ell}^{\ell} C_{\ell m} h_{\ell}^{(1)}(kr) Y_{\ell m}(\theta, \varphi)$$

where

$$C_{\ell m} = \frac{\rho_0 c k j_{\ell}(ka) - ik Z(\omega) j_{\ell}'(ka)}{i \rho_0 c h_{\ell}^{(1)}(ka) + Z(\omega) h_{\ell}^{(1)'}(ka)} h_{\ell}^{(1)}(kr_0) Y_{\ell m}^*(\theta_0, \varphi_0)$$

in which a prime denotes a spatial derivative.

#### Appendix B: Reflection of a Point Source by a Lined Plane

In this appendix, an analytical solution for a point-source reflection by an infinite flat surface with impedance boundary condition in the frequency domain is derived following a time-domain analytical solution found in Ref. [27]. Assume that the scattering surface is located at z = 0 and the point source is located at  $r_0 = (x_0, y_0, z_0), z_0 > 0$ . By the Weyl identity [28], the frequency-domain solution for the wave equation by a point source is expressed in plane waves as follows:

$$\begin{split} \hat{p}_{\text{inc}} &= \frac{e^{ik|\boldsymbol{r}-\boldsymbol{r}_0|}}{4\pi|\boldsymbol{r}-\boldsymbol{r}_0|} \\ &= \frac{i}{8\pi^2} \int_{-\infty}^{\infty} \int_{-\infty}^{\infty} \frac{\exp[i(k_x(x-x_0)+k_y(y-y_0)+\gamma|z-z_0|)]}{\gamma} \mathrm{d}k_x \mathrm{d}k_y \end{split}$$

where 
$$\gamma = \sqrt{k^2 - k_x^2 - k_y^2}$$
.

The time dependency is assumed to be  $e^{-i\omega t}$ , and a dispersion relation  $\omega = ck$  is assumed for the case without mean flow. Let the plane wave incident on the lined surface, denoted by a tilde

$$\tilde{p}_{\text{inc}} = A_{\text{inc}} \exp[i(k_x(x - x_0) + k_y(y - y_0) - \gamma(z - z_0))]$$
 (B1)

Further, the plane wave reflected by the surface at z = 0 is expressed as

$$\tilde{p}_{\text{ref}} = A_{\text{ref}} \exp[i(k_x(x - x_0) + k_y(y - y_0) + \gamma(z + z_0))]$$
 (B2)

Adding Eqs. (B1) and (B2) results in a total field such that  $\tilde{p}=\tilde{p}_{\rm inc}+\tilde{p}_{\rm ref}$  in Eq. (B3):

$$\tilde{p} = A_{\text{inc}} \exp[i(k_x(x - x_0) + k_y(y - y_0) - \gamma(z - z_0))] + A_{\text{ref}} \exp[i(k_x(x - x_0) + k_y(y - y_0) + \gamma(z + z_0))]$$
(B3)

The impedance boundary condition of Eq. (14) is applied at z = 0:

$$\begin{split} Z &= \frac{i\rho_0 c k (A_{\text{inc}} + A_{\text{ref}}) \exp[i(k_x (x - x_0) + k_y (y - y_0) + \gamma(z_0))]}{i\gamma (A_{\text{inc}} - A_{\text{ref}}) \exp[i(k_x (x - x_0) + k_y (y - y_0) + \gamma(z_0))]} \\ &= \frac{\rho_0 c k (A_{\text{inc}} + A_{\text{ref}})}{\gamma (A_{\text{inc}} - A_{\text{ref}})} \end{split}$$

By letting  $A = A_{\text{ref}}/A_{\text{inc}}$ , it is straightforward to show that  $A = (\gamma Z - \rho_0 ck)/(\gamma Z + \rho_0 ck)$ . Hence, the reflected wave of the point source is given by  $\hat{p}_{\text{ref}}$ :

$$\hat{p}_{\text{ref}} = \frac{i}{8\pi^2} \times \int_{-\infty}^{\infty} \int_{-\infty}^{\infty} \frac{A \exp[i(k_x(x-x_0) + k_y(y-y_0) + \gamma(z+z_0))]}{\gamma} dk_x dk_y$$

For convenience of numerical evaluation, as in Ref. [27], a change of variables from  $(k_x, k_y)$  to (u, v) is introduced such that  $k_x = u \cos v$  and  $k_y = u \sin v$ . This change of variables gives

where  $\gamma = \sqrt{k^2 - k_x^2 - k_y^2} = \sqrt{k^2 - u^2}$ . Further simplifications yield

$$\int_0^{2\pi} \exp[iu(\cos v(x - x_0) + \sin v(y - y_0))] dv$$

$$= \int_0^{2\pi} \exp[iur'\cos(v - \theta')] dv = 2\pi J_0(ur')$$

such that  $x - x_0 = r' \cos \theta'$ ,  $y - y_0 = r' \sin \theta'$ , and  $J_0$  is a Bessel function of the first kind. Hence, the equation for  $\hat{p}_{ref}$  is shown as follows:

$$\hat{p}_{\text{ref}} = \frac{i}{4\pi} \int_0^\infty \frac{A \exp[i\gamma(z+z_0)]}{\gamma} J_0(ur') u \, du$$

Furthermore, by considering a change of variables for 0 < u < k  $(\xi = (\gamma/k), u = k\sqrt{1-\xi^2})$  and a change of variables for  $k < u < \infty$   $(\xi = -(i\gamma/k), u = k\sqrt{1+\xi^2})$ , the following analytical expression is obtained for the reflected wave:

$$\hat{p}_{\text{ref}} = \frac{ik}{4\pi} \int_0^1 A(\xi) \exp[ik\xi(z+z_0)] J_0(kr'\sqrt{1-\xi^2}) \,d\xi + \frac{k}{4\pi} \int_0^\infty A(i\xi) \exp[-k\xi(z+z_0)] J_0(kr'\sqrt{1+\xi^2}) \,d\xi$$

in which  $A(\xi) = (\xi Z - \rho_0 c)/(\xi Z + \rho_0 c)$  and  $A(i\xi) = (i\xi Z - \rho_0 c)/(i\xi Z + \rho_0 c)$ .

# Acknowledgments

F. Q. Hu and M. E. Rodio were supported by a NASA Cooperative Agreement, NNX11AI63A. M. E. Rodio was also supported in part by a Virginia Space Grant Consortium Graduate Fellowship as part of her doctoral program. This work used the computational resources at the Old Dominion University Information Technology Services Turing Cluster and the Extreme Science and Engineering Discovery Environment, which is supported by the National Science Foundation, grant number OCI-1053575.

#### References

- [1] Ffowcs Williams, J., and Hawkings, D., "Sound Generation by Turbulence and Surfaces in Arbitrary Motion," *Philosophical Transactions of the Royal Society of London, Series A: Mathematical and Physical Sciences*, Vol. 264, No. 1151, 1969, pp. 321–342. https://doi.org/10.1098/rsta.1969.0031
- [2] Farassat, F., and Myers, M., "Extension of Kirchhoff's Formula to Radiation from Moving Surfaces," *Journal of Sound and Vibration*, Vol. 123, No. 3, 1988, pp. 451–460, https://ui.adsabs.harvard.edu/link\_ gateway/1988 JSV . . . 123.451F/. https://doi.org/10.1016/S0022-460X(88)80162-7
- [3] Morse, P., and Ingard, K., Theoretical Acoustics, 1st ed., Princeton Univ. Press, Princeton, NJ, 1986, Chap. 8.
- [4] Myers, M., and Hausmann, J., "Computation of Acoustic Scattering from a Moving Rigid Surface," *Journal of the Acoustical Society of America*, Vol. 91, No. 5, 1992, pp. 2594–2605. https://doi.org/10.1121/1.402996
- [5] Hu, F., Pizzo, M., and Nark, D., "On a Time Domain Boundary Integral Equation Formulation for Acoustic Scattering by Rigid Bodies in Uniform Mean Flow," *Journal of the Acoustical Society of America*,

$$\begin{split} \hat{p}_{\text{ref}} &= \frac{i}{8\pi^2} \int_0^{2\pi} \int_0^{\infty} \frac{A \exp[i(k_x(x-x_0) + k_y(y-y_0) + \gamma(z+z_0))]}{\gamma} u \, \mathrm{d}u \, \mathrm{d}v \\ &= \frac{i}{8\pi^2} \int_0^{2\pi} \int_0^{\infty} \frac{A \exp[i(u\cos v(x-x_0) + u\sin v(y-y_0) + \sqrt{k^2 - u^2}(z+z_0))]}{\gamma} u \, \mathrm{d}u \, \mathrm{d}v \end{split}$$

- Vol. 142, No. 6, 2017, pp. 3624–3636. https://doi.org/10.1121/1.5017734
- [6] Rynne, B., and Smith, P., "Stability of Time Marching Algorithms for the Electric Field Integral Equation," *Journal of Electromagnetic Waves* and Applications, Vol. 4, No. 12, 1990, pp. 1181–1205. https://doi.org/10.1163/156939390X00762
- [7] Burton, A., and Miller, G., "The Application of Integral Equation Methods to the Numerical Solution of Some Exterior Boundary-Value Problems," *Proceedings of the Royal Society of London, Series A: Mathematical and Physical Sciences*, Vol. 323, No. 1553, 1971, pp. 201–210. https://doi.org/10.1098/rspa.1971.0097
- [8] Ergin, A., Shanker, B., and Michielssen, E., "Analysis of Transient Wave Scattering from Rigid Bodies Using a Burton-Miller Approach," *Jour-nal of the Acoustical Society of America*, Vol. 106, No. 5, 1999, pp. 2396–2404. https://doi.org/10.1121/1.428076
- [9] Chappell, D., Harris, P., Henwood, D., and Chakrabarti, R., "A Stable Boundary Element Method for Modeling Transient Acoustic Radiation," *Journal of the Acoustical Society of America*, Vol. 120, No. 1, 2006, pp. 74–80. https://doi.org/10.1121/1.2202909
- [10] Rodio, M., Hu, F., and Nark, D., "Investigating the Numerical Stability of Multiple Broadband Impedance Boundary Conditions for Time-Domain Boundary Element Methods," 26th AIAA/CEAS Aeroacoustics Conference (AIAA Aviation 2020 Forum), AIAA Paper 2020-2547, June 2020. https://doi.org/10.2514/6.2020-2547
- [11] Motsinger, R., and Kraft, R., "Design and Performance of Duct Acoustic Treatment," Aeroacoustics of Flight Vehicles, Theory and Practice, NASA Langley Research Center, Hampton, VA, 1995, Chap. 14.
- [12] Li, X., Li, X., and Tam, C., "Improved Multipole Broadband Time-Domain Impedance Boundary Condition," *AIAA Journal*, Vol. 50, No. 4, 2012, pp. 980–984. https://doi.org/10.2514/1.J051361
- [13] Reymen, Y., Baelmans, M., and Desmet, W., "Efficient Implementation of Tam and Auriault's Time-Domain Impedance Boundary Condition," *AIAA Journal*, Vol. 46, No. 9, 2008, pp. 2368–2376. https://doi.org/10.2514/1.35876
- [14] Dragna, D., Pineau, P., and Blanc-Benon, P., "A Generalized Recursive Convolution Method for Time-Domain Propagation in Porous Media," *Journal of the Acoustical Society of America*, Vol. 138, No. 2, 2015, pp. 1030–1042. https://doi.org/10.1121/1.4927553
- [15] Troian, R., Dragna, D., Bailly, C., and Galland, M.-A., "Broadband Liner Impedance Eduction for Multimodal Acoustic Propagation in the Presence of a Mean Flow," *Journal of Sound and Vibration*, Vol. 392, March 2017, pp. 200–216. https://doi.org/10.1016/j.jsv.2016.10.014
- [16] Fung, K.-Y., and Ju, H., "Time-Domain Impedance Boundary Conditions for Computational Acoustics and Aeroacoustics," *International*

- Journal of Computational Fluid Dynamics, Vol. 18, No. 6, 2004, pp. 503–511.
- https://doi.org/10.1080/10618560410001673515
- [17] Rienstra, S., "Impedance Models in Time Domain, Including the Extended Helmholtz Resonator Model," 12th AIAA/CEAS Aeroacoustics Conference, AIAA Paper 2006-2686, May 2006. https://doi.org/10.2514/6.2006-2686
- [18] Meyer, W., Bell, W., Zinn, B., and Stallybrass, M., "Boundary Integral Solutions of Three Dimensional Acoustic Radiation Problems," *Journal* of Sound and Vibration, Vol. 59, No. 2, 1978, pp. 245–262. https://doi.org/10.1016/0022-460X(78)90504-7
- [19] Smith, P., "Instabilities in Time Marching Methods for Scattering: Cause and Rectification," *Electromagnetics*, Vol. 10, No. 4, 1990, pp. 439–451. https://doi.org/10.1080/02726349008908256
- [20] Butcher, J., Numerical Methods for Ordinary Differential Equations, 3rd ed., Wiley, New York, 2016, Chap. 4.
- [21] Golub, G., and Van Loan, C., *Matrix Computations*, 4th ed., Johns Hopkins Univ. Press, Baltimore, 2013, Chap. 7.
- [22] Nark, D., Jones, M., and Piot, E., "Assessment of Axial Wave Number and Mean Flow Uncertainty on Acoustic Liner Impedance Eduction," 24th AIAA/CEAS Aeroacoustics Conference, AIAA Paper 2018-3444, June 2018. https://doi.org/10.2514/6.2018-3444
- [23] Dodson, S., Walker, S., and Bluck, M., "Implicitness and Stability of Time Domain Integral Equation Scattering Analyses," *Applied Computational Electromagnetics Society Journal*, Vol. 13, No. 3, Nov. 1998, pp. 291–301.
- [24] Pizzo, M., Hu, F., and Nark, D., "Simulation of Sound Absorption by Scattering Bodies Treated with Acoustic Liners Using a Time-Domain Boundary Element Method," 24th AIAA/CEAS Aeroacoustics Conference, AIAA Paper 2018-3456, June 2018. https://doi.org/10.2514/6.2018-3456
- [25] Rodio, M., Hu, F., and Nark, D., "Investigating the Numerical Stability of a Time-Domain Boundary Integral Equation with Impedance Boundary Condition for Simulating Sound Absorption of Lined Bodies," 25th AIAA/CEAS Aeroacoustics Conference, AIAA Paper 2019-2416, May 2019. https://doi.org/10.2514/6.2019-2416
- [26] Bowman, J., Senior, T., and Uslenghi, P., Electromagnetic and Acoustic Scattering by Simple Shapes, 1st ed., Hemisphere, New York, 1987, Chap. 10.
- [27] Zheng, S., and Zhuang, M., "Three-Dimensional Benchmark Problem for Broadband Time-Domain Impedance Boundary Conditions," AIAA Journal, Vol. 42, No. 2, 2004, pp. 405–407. https://doi.org/10.2514/1.9102
- [28] Jackson, J., Classical Electrodynamics, 3rd ed., John Wiley & Sons, New York, 1999, Chap. 10.

D. Papamoschou Associate Editor